

New Architecture for High-Efficiency Polymer Photovoltaic Cells Using Solution-Based Titanium Oxide as an Optical Spacer**

By Jin Young Kim, Sun Hee Kim, Hyun-Ho Lee, Kwanghee Lee,* Wanli Ma, Xiong Gong, and Alan J. Heeger

Photovoltaic cells based on polymer:fullerene composites continue to be of interest as potential sources of renewable electrical energy.^[1–4] In particular, because of the advantages implied for polymer-based electronics, including low-cost fabrication in large areas and low weight on flexible substrates, efficient “plastic” solar cells would have a major impact. Although encouraging progress has been made in recent years, with 3–4 % power-conversion efficiencies^[5,6] and, more recently, power-conversion efficiencies approaching 5 %^[7,8] reported under AM 1.5 (AM: air mass) illumination, this efficiency is not sufficient to meet realistic specifications for commercialization. The need to improve the light-to-electricity conversion efficiency requires the implementation of new materials and the exploration of new device architectures.

Polymer-based photovoltaic cells are thin-film devices fabricated in the metal-insulator-metal configuration sketched in Figure 1a. The absorbing and charge-separating bulk-heterojunction layer with a thickness of approximately 100 nm is sandwiched between two charge-selective electrodes; a transparent bilayer electrode comprising poly(3,4-ethylenedioxythiophene):polystyrene sulfonic acid (PEDOT:PSS) on indium tin oxide (ITO) glass for collecting the holes and a lower-work-function metal (here, Al) for collecting the electrons. The work-function difference between the two electrodes provides a built-in potential that breaks the symmetry, thereby providing a driving force for the photogenerated electrons and holes toward their respective electrodes.

Because of optical interference between the incident (from the ITO side) and back-reflected light, the intensity of the light is zero at the metallic (Al) electrode; Figure 1a shows a schematic representation of the spatial distribution of the squared optical electric-field strength.^[9–11] Thus, a relatively large fraction of the active layer is in a dead-zone in which the photogeneration of carriers is significantly reduced. Moreover, this effect causes more electron-hole pairs to be produced near the ITO/PEDOT:PSS electrode, a distribution which is known to reduce the photovoltaic conversion efficiency.^[12,13] This “optical interference effect” is especially important for thin-film structures where layer thicknesses are comparable to the absorption depth and the wavelength of the incident light, as is the case for photovoltaic cells fabricated from semiconducting polymers.

In order to overcome these problems, one might simply increase the thickness of the active layer to absorb more light. Because of the low mobility of the charge carriers in the polymer:C₆₀ composites, however, the increased internal resistance of thicker films will inevitably lead to a reduced fill factor.

An alternative approach is to change the device architecture with the goal of spatially redistributing the light intensity inside the device by introducing an optical spacer between the active layer and the Al electrode as sketched in Figure 1a.^[11] Although this revised architecture would appear to solve the problem, the prerequisites for an ideal optical spacer limit the choice of materials: the layer must be a good acceptor and an electron-transport material with a conduction band edge lower in energy than that of the lowest unoccupied molecular orbital (LUMO) of C₆₀; the LUMO must be above (or close to) the Fermi energy of the collecting metal electrode; and it must be transparent to light with wavelengths within the solar spectrum.

Titanium dioxide is a promising candidate as an electron acceptor and transport material, as confirmed by its use in dye-sensitized cells,^[14,15] hybrid polymer/TiO₂ cells,^[16–18] and multilayer Cu-phthalocyanine/dye/TiO₂ cells.^[11,19] Typically, however, crystalline TiO₂ is used, either in the anatase phase or the rutile phase, both of which require treatment at temperatures ($T > 450$ °C) that are inconsistent with the device architecture shown in Figure 1; the polymer:C₆₀ composite cannot survive such high temperatures. We have used a solution-based sol-gel process to fabricate a titanium oxide (TiO_x) layer on top of the polymer:fullerene active layer (Fig. 1b). By introducing the TiO_x optical spacer, we demonstrate poly-

[*] Prof. K. Lee, Dr. J. Y. Kim,^[+] S. H. Kim, H.-H. Lee
Department of Physics
Pusan National University
Busan 609-735 (Korea)
E-mail: kwhlee@pusan.ac.kr

W. Ma, Dr. X. Gong, Prof. A. J. Heeger
Center for Polymers and Organic Solids
University of California at Santa Barbara
Santa Barbara, CA 93106-5090 (USA)

[+] Present address: Center for Polymers and Organic Solids, University of California at Santa Barbara, Santa Barbara, CA 93106-5090, USA.

[**] We thank Prof. Se Young Jeong for his help in preparing the titanium oxide material. The research at UCSB was supported by Konarka Technologies (Lowell, MA) and by the Air Force Office of Scientific Research, AFOSR, under FA9550-05-0139. The research at Pusan National University (Busan, Korea) was supported by the National Program for Nanoscience and Technology of the Ministry of Science and Technology of Korea (M1-0214-00-0077).

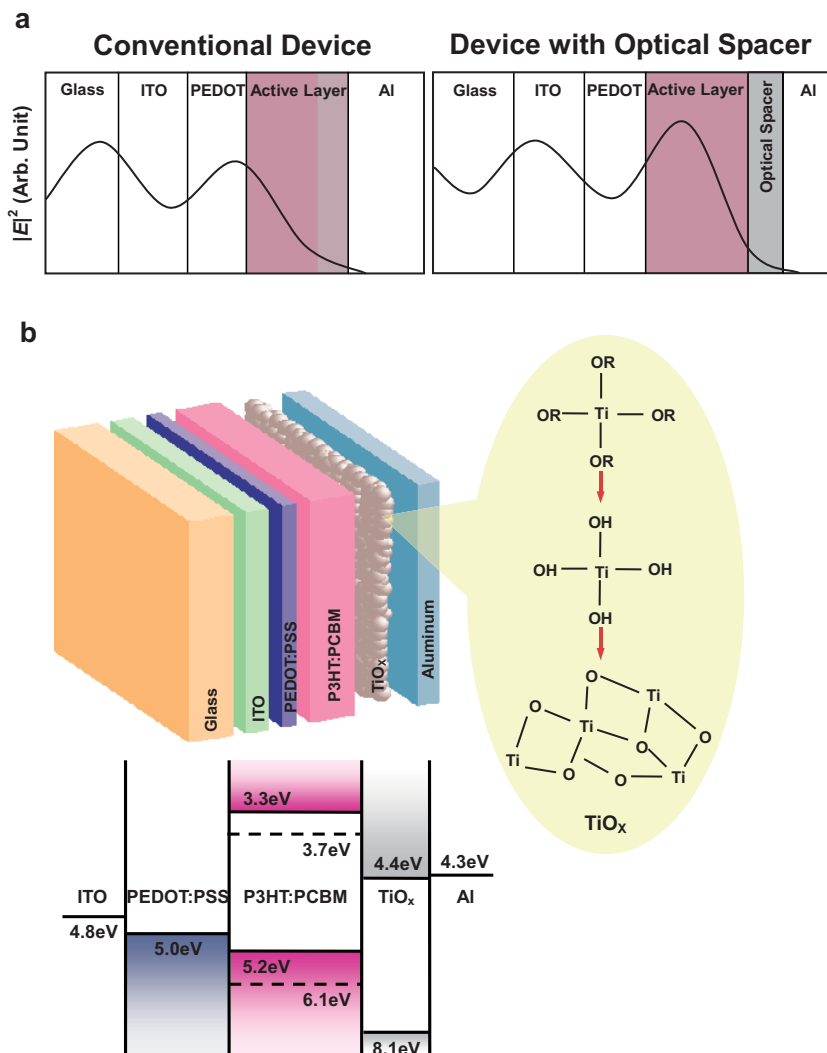


Figure 1. a) Schematic representation of the spatial distribution of the squared optical electric field strength $|E|^2$ inside the devices with a structure of ITO/PEDOT/active layer/Al (left) and ITO/PEDOT/active layer/optical spacer/Al (right). ITO: indium tin oxide; PEDOT: poly(3,4-ethylenedioxythiophene). b) Schematic illustration of the device structure with a brief flow chart of the steps involved in the preparation of the TiO_x layer. The energy levels of the single components of photovoltaic cell are also shown. P3HT: poly(3-hexylthiophene); PCBM: [6,6]-phenyl C_{61} -butyric acid methyl ester.

mer photovoltaic cells with power-conversion efficiencies that are increased by approximately 50 % compared to similar devices fabricated without the optical spacer.

Dense TiO_x films were prepared using a TiO_x precursor solution, as described in detail in the Experimental section. The precursor solution was spin-cast in air on top of the polymer:fullerene composite layer with a thickness of around 30 nm. Subsequently, during 1 h in air at room temperature, the precursor converted to TiO_x by hydrolysis. The sample was then heated at 150 °C for 10 min inside a glove box filled with nitrogen. As shown in Figure 2a, the resulting TiO_x films are transparent and smooth with surface features smaller than a few nanometers.

Since the TiO_x layer was deposited at room temperature and treated at 150 °C (far below the crystallization temperatures to the anatase or rutile phases, $T_c \geq 450$ °C), the film is amorphous as confirmed by X-ray diffraction (XRD) (Fig. 2b). The typical XRD peaks of the anatase crystalline form appear only after sintering the spin-cast films at 500 °C for 2 h as shown in Figure 2b. Analysis by X-ray photoelectron spectroscopy (XPS) reveals an oxygen deficiency at the surface of the thin film samples with a Ti:O ratio of 42.1:56.4 (in percent); hence, we designate the composition as TiO_x .

In spite of the amorphous nature of the TiO_x layer, the physical properties are excellent. Time-of-flight measurements on these TiO_x films indicate that the electron mobility (μ_e) is approximately $1.7 \times 10^{-4} \text{ cm}^2 \text{ V}^{-1} \text{ s}^{-1}$, which is somewhat higher than mobility values obtained from amorphous oxide films prepared by typical sol-gel processes. The absorption spectrum of the film shows a well-defined absorption edge at $E_g \approx 3.7 \text{ eV}$ as shown in Figure 2c. Using optical absorption and cyclic voltammetry (CV) data, the energies of the bottom of the conduction band (LUMO) and the top of the valence band (highest occupied molecular orbital, HOMO) of the TiO_x material were determined (see Fig. 1b). This energy-level diagram demonstrates that the TiO_x layer satisfies the electronic-structure requirements of the optical spacer.

Utilizing this TiO_x layer as the optical spacer, we fabricated donor/acceptor composite photovoltaic cells using the phase-separated “bulk heterojunction” material comprising poly(3-hexylthiophene) (P3HT) as the electron donor and the fullerene derivative [6,6]-phenyl C_{61} -butyric acid methyl ester (PCBM) as the acceptor. The device structure is shown in Figure 1b.

Figure 3a compares the incident photon-to-current collection efficiency (IPCE) spectrum of devices fabricated with and without the TiO_x optical spacer. The IPCE is defined as the number of photogenerated charge carriers contributing to the photocurrent per incident photon. The conventional device (without the TiO_x layer) shows the typical spectral response of P3HT:PCBM composites with a maximum IPCE of ~60 % at 500 nm, consistent with previous studies.^[3–7] For the device with the TiO_x optical spacer, the results demonstrate a substantial enhancement of ~40 % in the IPCE over the entire excitation spectral range.

We attribute this enhancement to increased absorption in the bulk heterojunction layer as a result of the TiO_x optical

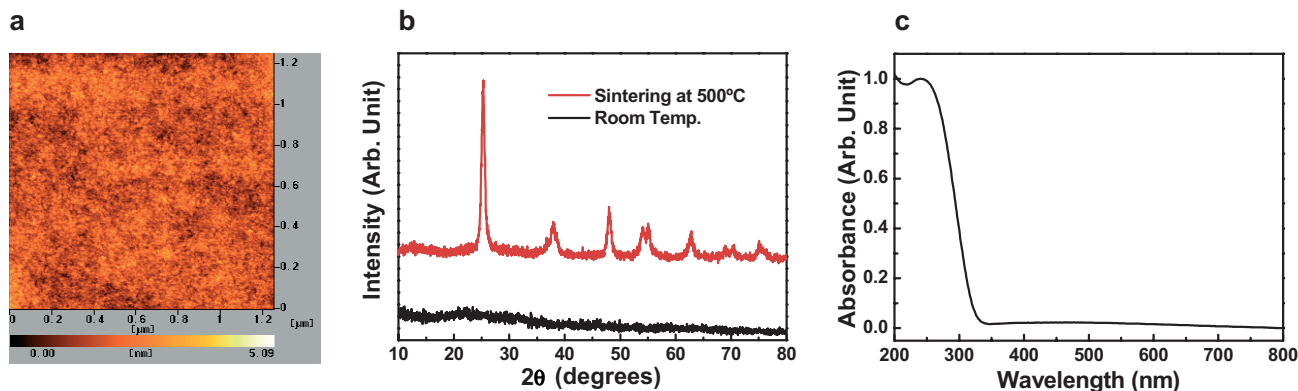


Figure 2. a) Surface morphology of the TiO_x film observed by tapping mode atomic force microscopy. b) X-ray diffraction patterns of TiO_x at room temperature and TiO_2 film calculated at 500°C . c) Absorption spectrum of the spin-coated TiO_x film.

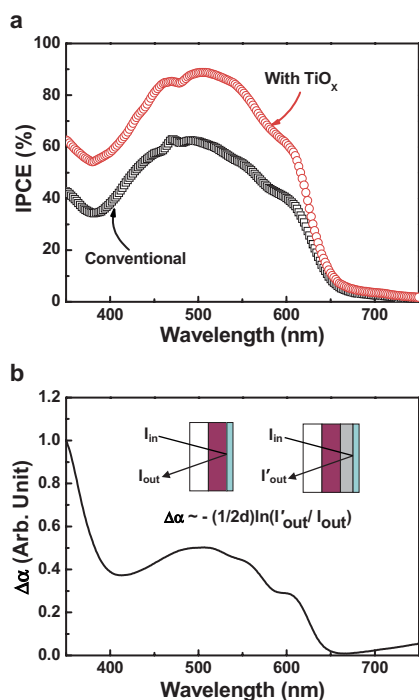


Figure 3. a) Incident monochromatic photon-to-current collection efficiency spectra for the two devices with and without the TiO_x optical spacer layer. b) The change in the absorption spectrum ($\Delta\alpha$) resulting from the addition of the optical spacer as given in Equation 1. The inset is a schematic of the optical beam path in the samples; the variables are defined in the text.

spacer; the increased photogeneration of charge carriers results from the spatial redistribution of the light intensity.

In order to further clarify the role of the TiO_x layer, we measured the reflectance spectrum from a “device” with a glass/P3HT:PCBM/ TiO_x /Al geometry using a glass/P3HT:PCBM/Al “device” as the reference (the P3HT:PCBM composite film thickness, d , was about 100 nm in both). Note that the ITO/PEDOT layers were omitted to avoid any com-

plication arising from the conducting layers. Since the two “devices” are identical except for the TiO_x optical spacer, comparison of the reflectance yields information on the additional absorption, $\Delta\alpha(\omega)$, in the P3HT:PCBM composite film as a result of the spatial redistribution of the light intensity by the TiO_x layer^[20]

$$\Delta\alpha(\omega) \approx -(1/2d)\ln[I_{\text{out}}'(\omega)/I_{\text{out}}(\omega)] \quad (1)$$

where $I_{\text{out}}'(\omega)$ is the intensity of the reflected light from the device with the optical spacer and $I_{\text{out}}(\omega)$ is the intensity of the reflected light from an identical device without the optical spacer. The data demonstrate a clear increase in absorption over the spectral region of the interband transitions, $\Delta\alpha(\omega) > 0$. Since the spectral features of the P3HT:PCBM absorption are evident in $\Delta\alpha(\omega)$, the increased absorption arises from a better match of the spatial distribution of the light intensity to the position of the P3HT:PCBM composite film. We conclude that the higher absorption is caused by the TiO_x layer as an optical spacer as sketched in Figure 1a. As a result, the TiO_x optical spacer increases the number of carriers per incident photon collected at the electrodes.

As shown in Figure 4a, the enhancement in the device efficiency that results from the optical spacer can be directly observed in the current-density versus voltage (J - V) characteristics under monochromatic illumination with an intensity of 25 mW cm^{-2} at a wavelength of 532 nm. The conventional device (without the TiO_x layer) shows a typical photovoltaic response with device performance comparable to that reported in previous studies; the short-circuit current (I_{sc}) is 8.4 mA cm^{-2} , the open-circuit voltage (V_{oc}) is 0.60 V, and the fill factor (FF) is 0.40. These values correspond to a power-conversion efficiency ($\eta_e = I_{\text{sc}} V_{\text{oc}} FF/P_{\text{inc}}$, where P_{inc} is the intensity of incident light) of 8.1%. For the device with the TiO_x layer, the results demonstrate substantially improved device performance; I_{sc} increases to 11.8 mA cm^{-2} , the FF increases slightly to 0.45, while V_{oc} remains at 0.60 V. The corresponding power-conversion efficiency is 12.6%, which corresponds

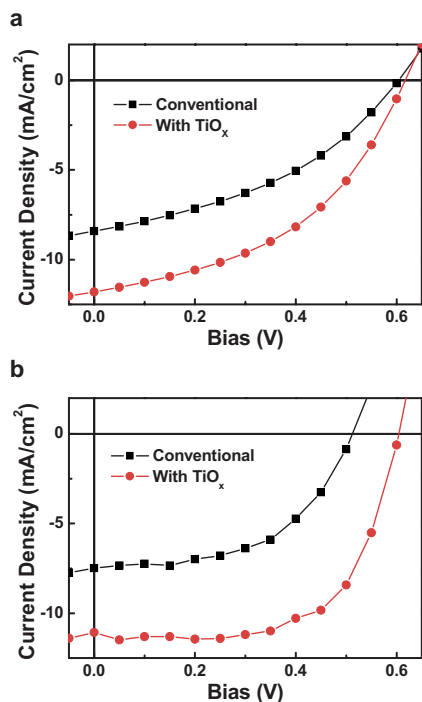


Figure 4. The current-density–voltage characteristics of polymer solar cells with (circles) and without (squares) the TiO_x optical spacer a) illuminated with an intensity of 25 mW cm^{-2} at 532 nm and b) under AM1.5 illumination from a calibrated solar simulator with an intensity of 90 mW cm^{-2} .

to an approximately 50 % increase in the device efficiency. Since the device efficiency is proportional to the product $I_{\text{sc}} V_{\text{oc}} FF$, most of the increase in the device efficiency results from the increased I_{sc} (~40 % increase in the device with the TiO_x layer) rather than V_{oc} or FF . This observation is in excellent agreement with the IPCE measurements.

The corresponding data obtained under AM1.5 illumination from a calibrated solar simulator with irradiation intensity of 90 mW cm^{-2} are shown in Figure 4b. In order to clarify the role of the TiO_x layer the devices (with and without the TiO_x layer) have been fabricated using exactly the same procedures and under exactly the same conditions, except for the TiO_x deposition. The device without the TiO_x layer again shows a typical photovoltaic response with device performance comparable to that reported in previous studies; $I_{\text{sc}} = 7.5 \text{ mA cm}^{-2}$, $V_{\text{oc}} = 0.51 \text{ V}$, $FF = 0.54$, and $\eta_e = 2.3 \%$. For the device with the TiO_x layer, the results demonstrate substantially improved performance; $I_{\text{sc}} = 11.1 \text{ mA cm}^{-2}$, $V_{\text{oc}} = 0.61 \text{ V}$, and $FF = 0.66$. The corresponding power-conversion efficiency is 5.0 %. Again, the increase in I_{sc} (~50 % increase for the TiO_x device) is the major contribution to the increase in the device efficiency, consistent with the IPCE measurements and with the results obtained from monochromatic illumination (Fig. 4a). The excellent consistency between the different measurements demonstrates that the TiO_x optical spacer contributes to the increase of the device efficiency by creating more photogenerated charge carriers in the bulk heterojunction layer, thereby increasing I_{sc} .

We note that the electron-collecting contact is changed in the new device architecture. First of all, two additional interfaces have been introduced ($\text{P3HT}:\text{PCBM}/\text{TiO}_x$ and TiO_x/Al). These interfaces might alter the charge-carrier concentration and could even cause reduced recombination. Although the effect of the TiO_x layer is consistent with the optical spacer concept (as demonstrated by Fig. 3), the effect of the TiO_x layer must be investigated more broadly to clarify the role of the altered electron-collecting contact. In particular, charge transport across these two additional interfaces has not yet been studied in detail.

The semiconducting polymer used in these studies, P3HT, has a relatively large energy gap (approximately 2 eV). As a result, approximately half of the energy in the solar spectrum is at wavelengths in the near IR at wavelengths too long to be absorbed. We anticipate that utilizing both a semiconducting polymer with an energy gap well matched to the solar spectrum and the optical spacer concept described here will result in polymer solar cells with greater than 10 % efficiency for conversion of sunlight to electricity. Low-cost plastic solar cells with power-conversion efficiencies approaching 10 % could have a major impact on the energy needs of our society.

Experimental

The sol–gel procedure for producing TiO_x is as follows: titanium(IV) isopropoxide ($\text{Ti}[\text{OCH}(\text{CH}_3)_2]_4$, Aldrich, 99.999 %, 10 mL) was prepared as a precursor and mixed with 2-methoxyethanol ($\text{CH}_3\text{OCH}_2\text{CH}_2\text{OH}$, Aldrich, 99.9+ %, 50 mL) and ethanolamine ($\text{H}_2\text{NCH}_2\text{CH}_2\text{OH}$, Aldrich, 99+ %, 5 mL) in a three-necked flask equipped with a condenser, a thermometer, and an argon-gas inlet/outlet. Then, the mixed solution was heated to 80°C for 2 h in a silicon-oil bath under magnetic stirring, followed by heating to 120°C for 1 h. The two-step heating (80 and 120°C) was then repeated. The typical TiO_x precursor solution was prepared in isopropyl alcohol.

The bulk-heterojunction solar cells using P3HT as the electron donor and PCBM as the acceptor were fabricated in the structure shown in Figure 1b. The details of the device fabrication (solvent, P3HT/PCBM ratio, and concentrations) have direct impact on the device performance.

Solvent: For achieving optimum performance, we used chlorobenzene as the solvent.

P3HT/PCBM Ratio and Concentration: The best device performance was achieved when the mixed solution had a P3HT/PCBM ratio of 1.0:0.8; i.e., with a concentration of P3HT (1 wt.-%) plus PCBM (0.8 wt.-%) in chlorobenzene.

Device Fabrication: Polymer solar cells were prepared according to the following procedure: The ITO-coated glass substrate was first cleaned with detergent, then ultrasonicated in acetone and isopropyl alcohol, and subsequently dried in an oven overnight. Highly conducting poly(3,4-ethylenedioxyethylenethiophene):polystyrene sulfonic acid (PEDOT:PSS, Baytron P) was spin-cast (5000 rpm) with a thickness of ~40 nm from aqueous solution (after passing through a $0.45 \mu\text{m}$ filter). The substrate was dried for 10 min at 140°C in air and then moved into a glove box for spin-casting the photoactive layer. The chlorobenzene solution composed of P3HT (1 wt.-%) plus PCBM (0.8 wt.-%) was then spin-cast at 700 rpm on top of the PEDOT layer. Then, the TiO_x precursor solution was spin-cast in air on top of the polymer:fullerene composite layer. Subsequently, during 1 h in air at room temperature, the precursor converted to TiO_x by hydrolysis. The sample was then heated at 150°C for 10 min inside a

glove box filled with nitrogen. Subsequently the device was pumped down in vacuum ($<10^{-7}$ torr; 1 torr \sim 133 Pa), and a \sim 100 nm thick Al electrode was deposited on top. The deposited Al electrode area defined the active area of the devices as 14.8 mm².

Calibration and Measurement: For calibration of our solar simulator, we first carefully minimized the mismatch of the spectrum (the simulating spectrum) obtained from the xenon lamp (150 W Oriol) and the solar spectrum using an AM1.5 filter. We then calibrated the light intensity using calibrated standard silicon photovoltaic (PV) solar cells traced to the National Renewable Energy Laboratory (NREL). Measurements were done with the solar cells inside the glove box by using a high-quality optical fiber to guide the light from the solar simulator (placed outside the glove box). Current density–voltage curves were measured with a Keithley 236 source measurement unit.

Received: August 31, 2005

Final version: November 15, 2005

-
- [1] N. S. Sariciftci, L. Smilowitz, A. J. Heeger, F. Wudl, *Science* **1992**, 258, 1474.
 - [2] G. Yu, J. Gao, J. C. Hummelen, F. Wudl, A. J. Heeger, *Science* **1995**, 270, 1789.
 - [3] C. J. Brabec, N. S. Sariciftci, J. C. Hummelen, *Adv. Funct. Mater.* **2001**, 11, 15.
 - [4] C. J. Brabec, *Sol. Energy Mater. Sol. Cells* **2004**, 83, 273.
 - [5] S. E. Shaheen, C. J. Brabec, N. S. Sariciftci, F. Padinger, T. Fromherz, J. C. Hummelen, *Appl. Phys. Lett.* **2001**, 78, 841.
 - [6] F. Padinger, R. Rittberger, N. S. Sariciftci, *Adv. Funct. Mater.* **2003**, 13, 85.
 - [7] W. Ma, C. Yang, X. Gong, K. Lee, A. J. Heeger, *Adv. Funct. Mater.* **2005**, 15, 1617.
 - [8] M. Reyes-Reyes, K. Kim, D. L. Carroll, *Appl. Phys. Lett.* **2005**, 87, 083 506.
 - [9] L. A. A. Pettersson, L. S. Roman, O. Inganäs, *J. Appl. Phys.* **1999**, 86, 487.
 - [10] T. Stübinger, W. Brütting, *J. Appl. Phys.* **2001**, 90, 3632.
 - [11] H. Hänsel, H. Zettl, G. Krausch, R. Kisselev, M. Thelakkat, H.-W. Schmidt, *Adv. Mater.* **2003**, 15, 2056.
 - [12] H. J. Snaith, N. C. Greenham, R. H. Friend, *Adv. Mater.* **2004**, 16, 1640.
 - [13] C. Melzer, E. J. Koop, V. D. Mihaletchi, P. W. M. Blom, *Adv. Funct. Mater.* **2004**, 14, 865.
 - [14] B. O'Regan, M. Grätzel, *Nature* **1991**, 353, 737.
 - [15] U. Bach, D. Lupo, P. Comte, J. E. Moser, F. Weissörtel, J. Salbeck, H. Spreitzer, M. Grätzel, *Nature* **1998**, 395, 583.
 - [16] A. C. Arango, L. R. Johnson, V. N. Bliznyuk, Z. Schlesinger, S. A. Carter, H.-H. Hörhold, *Adv. Mater.* **2000**, 12, 1689.
 - [17] A. J. Breeze, Z. Schlesinger, S. A. Carter, P. J. Brock, *Phys. Rev. B: Condens. Matter Mater. Phys.* **2001**, 64, 125 205.
 - [18] P. A. van Hal, M. M. Wienk, J. M. Kroon, W. J. H. Verhees, L. H. Slooff, W. J. H. van Gennip, P. Jonkheijm, R. A. J. Janssen, *Adv. Mater.* **2003**, 15, 118.
 - [19] M. Thelakkat, C. Schmitz, H.-W. Schmidt, *Adv. Mater.* **2002**, 14, 577.
 - [20] K. Lee, Y. Chang, J. Y. Kim, *Thin Solid Films* **2003**, 423, 131.
-